

## OBSERVATIONS OF THERMAL FLARE PLASMA WITH THE EUV VARIABILITY EXPERIMENT

HARRY P. WARREN<sup>1</sup>, JOHN T. MARISKA<sup>2</sup>, AND GEORGE A. DOSCHEK<sup>1</sup>

<sup>1</sup>Space Science Division, Naval Research Laboratory, Washington, DC 20375 and

<sup>2</sup>School of Physics, Astronomy, and Computational Sciences, George Mason University, 4400 University Drive, Fairfax VA 22030

*Draft version May 26, 2021*

### ABSTRACT

One of the defining characteristics of a solar flare is the impulsive formation of very high temperature plasma. The properties of the thermal emission are not well understood, however, and the analysis of solar flare observations is often predicated on the assumption that the flare plasma is isothermal. The EUV Variability Experiment (EVE) on the *Solar Dynamics Observatory* (SDO) provides spectrally resolved observations of emission lines that span a wide range of temperatures (e.g., Fe XV–Fe XXIV) and allow for thermal flare plasma to be studied in detail. In this paper we describe a method for computing the differential emission measure distribution in a flare using EVE observations and apply it to several representative events. We find that in all phases of the flare the differential emission measure distribution is broad. Comparisons of EVE spectra with calculations based on parameters derived from the *GOES* soft X-ray fluxes indicate that the isothermal approximation is generally a poor representation of the thermal structure of a flare.

*Subject headings:* Sun: corona

### 1. INTRODUCTION

It is widely believed that solar flares are powered by magnetic reconnection (e.g., Priest & Forbes 2002). How this energy is released over short time scales relative to magnetic diffusion is not well understood. Since a significant fraction of the energy released during a solar flare is ultimately radiated away, fully characterizing thermal emission and how it evolves with time is critical for providing strong observational constraints on theoretical models. During the past several decades flare observations have generally focused on either broad-band, soft X-ray measurements or high spectral resolution measurements of individual emission lines. Such observations have been unable to determine the full distribution of plasma temperatures in a flare and there have been only a few calculations of flare differential emission measure (DEM) distributions that extend to temperatures of 5 MK and lower (e.g., McTiernan et al. 1999; Dere & Cook 1979).

The launch of the EUV Variability Experiment (EVE, Woods et al. 2012) on the *Solar Dynamics Observatory* (SDO) provides a new opportunity to study thermal flare plasma. EVE is a spectral irradiance monitoring instrument that observes the full Sun at wavelengths between approximately 65 and 1050 Å with 1 Å spectral resolution and a 10 s cadence. The spectral coverage of EVE allows for the observation of flare emission lines in the 90–150 Å wavelength range, which has not been observed systematically for many decades (e.g., Kastner et al. 1974). Emission lines in this spectral range cover Fe XVIII to Fe XXIII and, in combination with observations of other emission lines in the EUV such as Fe XV 284.16 Å and Fe XXIV 192.04 Å, provide a complete description of thermal flare plasma at temperatures from 2 to 30 MK. Moreover, the Fe XXI lines in this wavelength range are sensitive to the electron density (Mason et al. 1979; Milligan et al. 2012) and provide information on the emission-measure-weighted density in the flare.

In this paper we describe a method for calculating the differential emission measure using EVE observations and illustrate the application of this method using several long duration events associated with coronal mass ejections. We focus on

two-ribbon, eruptive events because the magnetic geometry of the post-eruption arcade, a Y-type current sheet, appears to be consistent with the observations and provides perhaps the simplest environment in which to study magnetic reconnection in the solar atmosphere. Furthermore, two-ribbon flares provide an ideal way to test the hydrodynamics of loop evolution. The observations suggest that flare loops are heated impulsively leading to the evaporation of material into the corona, and subsequent cooling to lower temperatures. It remains to be seen, however, whether 1-D hydrodynamic simulations can accurately model the flow of mass and energy through the solar atmosphere in even this very simple case.

For the events we consider we find a relatively broad DEM during all phases of the flare. As expected, the highest temperature emission is observed during the rise phase and at the peak of the event. During the decay phase of the flare the magnitude of the emission measure decays exponentially but the peak temperature declines very slowly. We also find that the shape of the temperature distribution remains relatively constant as the flare decays over many hours, suggesting that plasma temperature is relatively insensitive to the magnitude of the energy released by the magnetic reconnection process.

For these observations we also compute the isothermal temperature and emission measure from the ratio of the *GOES* soft X-ray fluxes and use these parameters to infer the expected EVE spectrum. These comparisons show that the differential emission measure distribution reproduces the observations at EUV wavelengths much better than an isothermal model. Single temperature fits are often used in the analysis and interpretation of solar flare observations (e.g., Sui & Holman 2003).

### 2. OBSERVATIONS

EVE is actually a collection of instruments designed to measure the solar irradiance at many EUV wavelengths. In this work we will consider observations from the Multiple EUV Grating Spectrograph A (MEGS-A), which is a grazing incidence spectrograph that observes in the 50 to 370 Å wavelength range. MEGS-A has a spectral resolution of approximately 1 Å and an observing cadence of 10 s. For more

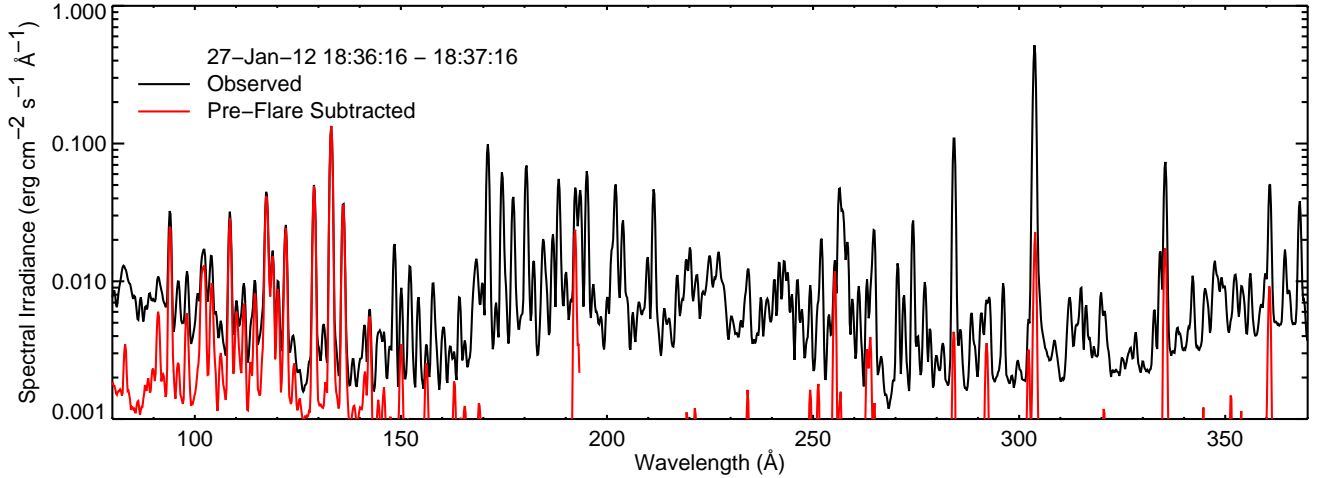


FIG. 1.— EVE observations of the solar spectral irradiance near the peak of an X1.7 flare that occurred on 2012 January 27. Both the observed and pre-flare subtracted spectra are shown. Emission lines from Fe XV to Fe XXIV are evident in the flare spectrum.

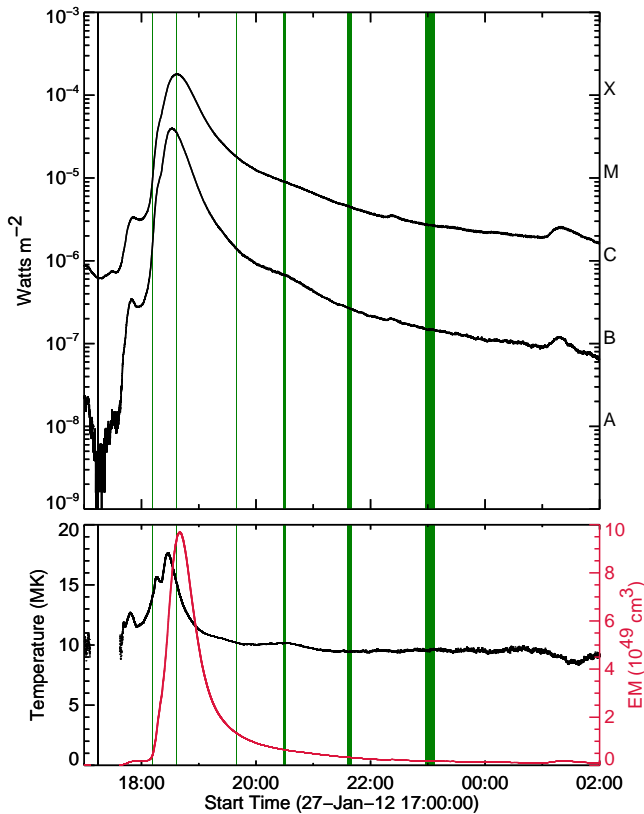


FIG. 2.— *GOES* observations of the 2012 January 27 X1.7 flare. The top panel shows the *GOES* soft X-ray 0.5–4 and 1–8 Å fluxes as a function of time. The vertical lines indicate intervals selected for determining the background for both *EVE* and *GOES* as well as other times of interest during the rise, peak, and decay of the flare. The bottom panel shows the isothermal temperature and emission measure derived from the *GOES* fluxes.

detail see Woods et al. (2012).

An example *EVE* spectrum from the peak of the X1.7 flare that occurred on 2012 January 27 between approximately 17 and 22 UT is shown in Figure 1. We will use this event to describe our analysis in detail and then consider other events more briefly. Figure 1 clearly shows the utility of the MEGS-A wavelength range for determining the properties of thermal

flare plasma. Observations between 90 and 150 Å, where we find some of the most intense emission lines from Fe XVIII–Fe XXIII, are a particularly rich source of diagnostics. Additionally, there are the strong Fe XXIV 192.04 and 255.10 Å flare lines within the MEGS-A wavelength range. Observations of Fe XV 284.16 Å and Fe XVI 335.41 Å provide information on lower temperature plasma.

For this work we also analyze observations from the soft X-ray monitors on the *Geostationary Operational Environmental Satellites (GOES)*, which provide spatially integrated fluxes in the 1–8 and 0.5–4 Å wavelength ranges at a 2 s cadence. These bandpasses have contributions from Fe XXV and Fe XXVI emission lines. These ions are formed at somewhat higher temperatures than the lines found in the MEGS-A wavelength range. Free-free continuum is also important at these wavelengths. Additional details on the *GOES* soft X-ray monitors can be found in Garcia (1994), White et al. (2005), and Aschwanden & Freeland (2012).

The *GOES* light curves for the 2012 January 27 X1.7 event are shown in Figure 2. We use the *GOES* light curves to identify various times of interest during the rise, peak, and decay of the flare. These six times are indicated on the light curves shown in Figure 2. For the analysis of both the *GOES* and *EVE* data background subtraction is necessary to isolate the contribution of the flare. For this we use a 60 s interval centered around the lowest observed flux in the *GOES* 0.5–4 Å channel during the 30 minutes preceding the peak of the flare. This time interval is also indicated in Figure 2.

Like *GOES*, *EVE* makes spatially unresolved observations. In contrast to *GOES*, the EUV irradiance is generally dominated by non-flare emission (see Figure 1). Also, at a spectral resolution of 1 Å, the vast majority of the flare lines in the EUV are blended with other lines formed at much cooler temperatures. To further complicate the analysis many of these lower temperature emission lines are unidentified and there is no atomic data for them (e.g., Testa et al. 2012). Given these constraints the best strategy is to remove the lower temperature emission by subtracting a pre-flare observation from the *EVE* measurements during the event. The primary risk in this approach is that the lower temperature emission will also evolve during the event. For example, for eruptive events dimming is often observed in emission lines formed around 1 MK

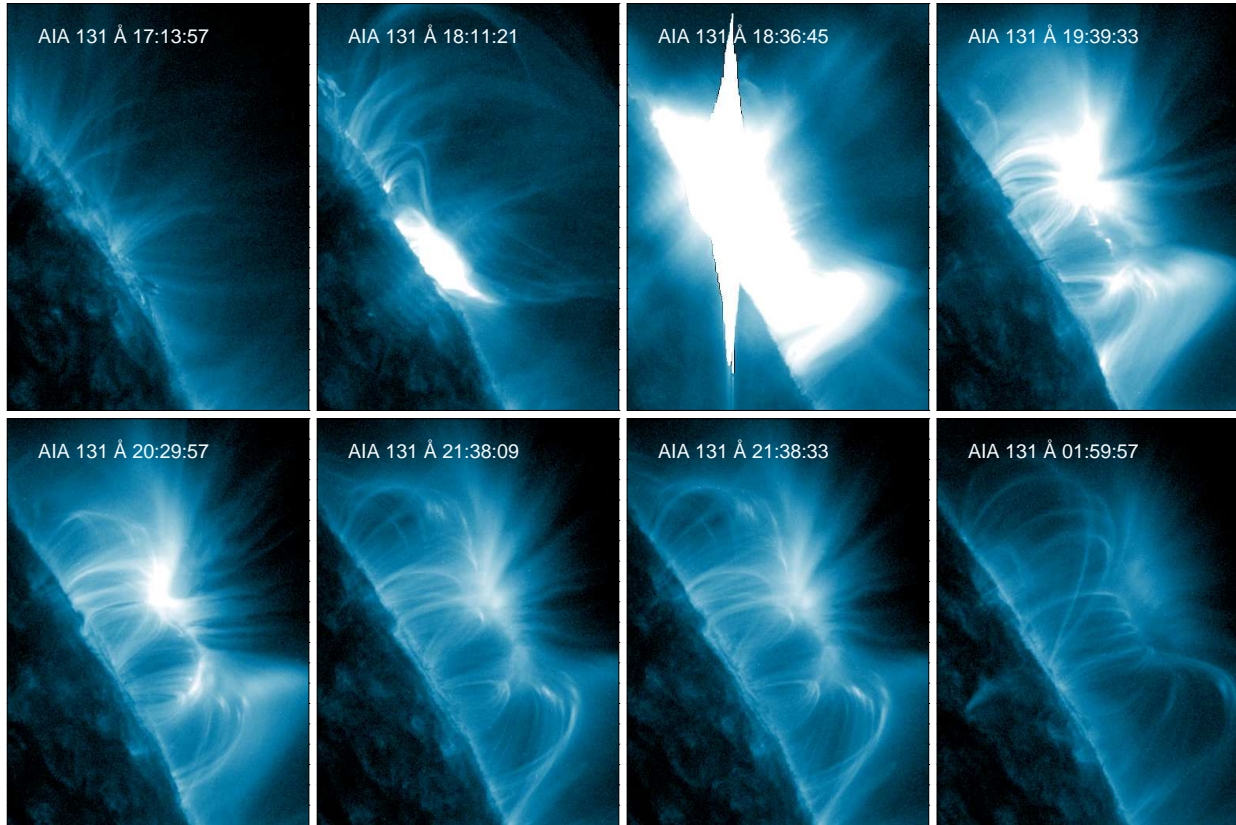


FIG. 3.— AIA 131 Å images from various times during the 27 January 2012 X1.7 flare and coronal mass ejection. All of the images shown here have the same logarithmic scaling. This AIA channel is sensitive to both high temperature flare plasma from Fe XXI 128.75 Å and lower temperature emission from Fe VIII emission lines.

(e.g., Gopalswamy & Hanaoka 1998), which would lead to an underestimate of flare emission.

To prepare the EVE observations for analysis we performed some additional processing to the calibrated level2 data. We first computed time-averaged EVE spectra for each of the time intervals indicated in Figure 2. We use the observed standard deviation in the irradiance measurements ( $\sigma_I$ ) to estimate the statistical uncertainty in each spectral bin,  $\sigma_{\bar{I}} = \sigma_I / \sqrt{N}$ , where  $N$  is the number of spectra in the average. We then subtracted the pre-flare, background spectrum from each of these spectra and propagate the errors in the usual way. The statistical uncertainties for the background subtracted flare irradiances are generally very small (approximately 1% at most wavelengths) and are likely to be dominated by systematic errors in the analysis, such as the assumption that the non-flare irradiance is constant during the event.

Both free-free and free-bound continuum emission has been observed during flares with EVE (Milligan et al. 2012), but to simplify our analysis we have chosen to remove it. To accomplish this we determine the lowest intensity in each 10 Å wavelength bin and subtract this from the observed spectrum. An example background subtracted spectrum from the peak of the X1.7 flare is shown in Figure 1.

Finally, to provide context for these observations we have investigated the images from the AIA instrument on *SDO* (Lemen et al. 2012). AIA is a set of multi-layer telescopes capable of imaging the full Sun at high spatial resolution (0.6'' pixels) and high cadence (typically 12 s). Images are available at 94, 131, 171, 193, 211, 304, and 335 Å. AIA images

are also available at UV and visible wavelengths, but they are not used in this analysis. The AIA 131 Å includes contributions from Fe XXI 128.75 Å and is particularly useful for flare observations. It also includes contributions from lower temperature emission lines. Figure 3 shows several images from the event. An animation of these data clearly shows an eruption followed by the formation of a classical post-flare loop arcade.

### 3. FLARE DENSITY AND EMISSION MEASURE

In this section we will determine the density and temperature evolution for the 2012 January 27 event. We will consider both the isothermal emission measure model that can be derived from the *GOES* observations as well as the DEM model that can be derived from EVE. Calculations of plasma emissivities, which form the basis of the temperature analysis, require information on the density so we begin with electron densities that can be inferred from the Fe XXI emission lines observed in the EVE spectra.

#### 3.1. Electron Densities

Most emission lines formed at flare temperatures are largely insensitive to the density and it is possible to compute the emission measure using any reasonable value. But, since observed intensity is very sensitive to the density, such measurements do provide an important constraint for hydrodynamic modeling. Anticipating this we consider the evolution of densities for this event.

As mentioned in the introduction, there are several emission lines in the 90 to 150 Å wavelength range from Fe XXI

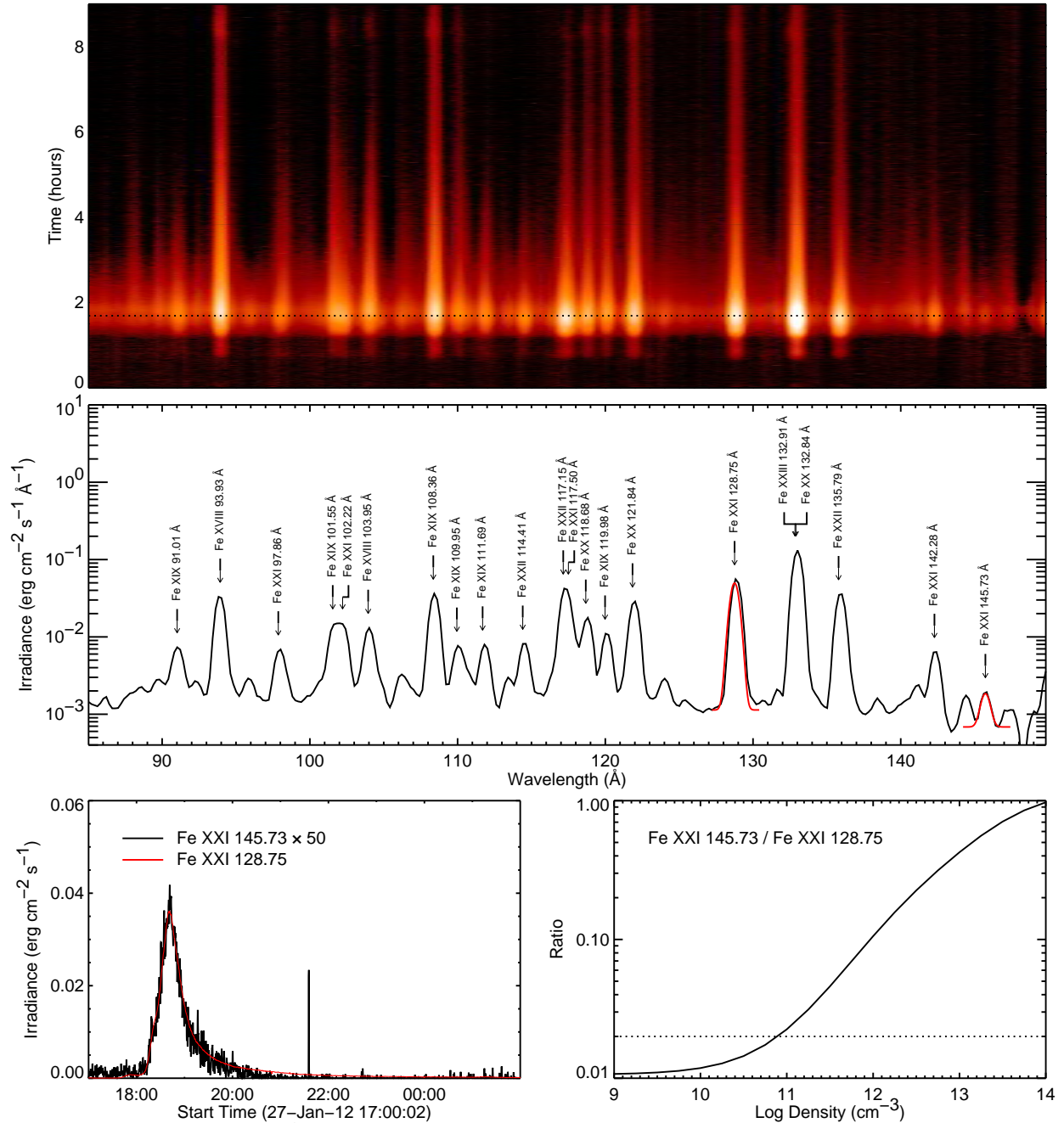


FIG. 4.— EVE observations of the 85–150 Å wavelength range for the X1.7 flare that occurred on January 27, 2012. The top panel shows the spectra as a function of time and wavelength. The middle panel shows the spectrum at the peak of the event with many of the most intense emission lines identified. A pre-flare spectrum has been subtracted from the observed irradiance during the flare. The peak intensities above the local continuum to estimate the total intensity of Fe XXI 128.75 and 145.72 Å. The bottom panels shown the evolution these lines. During most of the event the line ratio is approximately 0.02 corresponding to a density of  $10^{11} \text{ cm}^{-3}$ . This theoretical ratio was computed using the CHIANTI database.

that form density sensitive pairs (Mason et al. 1979). More recent theoretical calculations are available from the CHIANTI atomic physics database (e.g., Dere et al. 1997, 2009; Landi et al. 2012). The application of these ratios to the EVE data have been considered recently by Milligan et al. (2012). Their analysis suggests that the 145.73/128.75 Å ratio is the most useful. This ratio has a larger dynamic range than the (142.14+142.28)/128.75 Å ratio and is not as blended as 121.21/128.75 Å. For very large events all three ratios yield similar results. Following Milligan et al. (2012) we use the peak intensity above the local continuum as a proxy for the

total intensity. As is shown in Figure 4, the 145.73/128.75 Å ratio is approximately 0.02 over most of the event indicating an electron density of approximately  $10^{11} \text{ cm}^{-3}$ . The peak temperature of formation of Fe XXI is  $10^7 \text{ K}$  and we will assume a constant pressure of  $10^{18} \text{ K cm}^{-3}$  for these calculations.

We note that because of the weakness of the Fe XXI 145.73 Å lines, densities are only available near the peak of the event. The *GOES* light curves and the AIA images show flare emission extending to at least 2 UT on 2012 January 28. It is likely that the densities are lower during the decay and



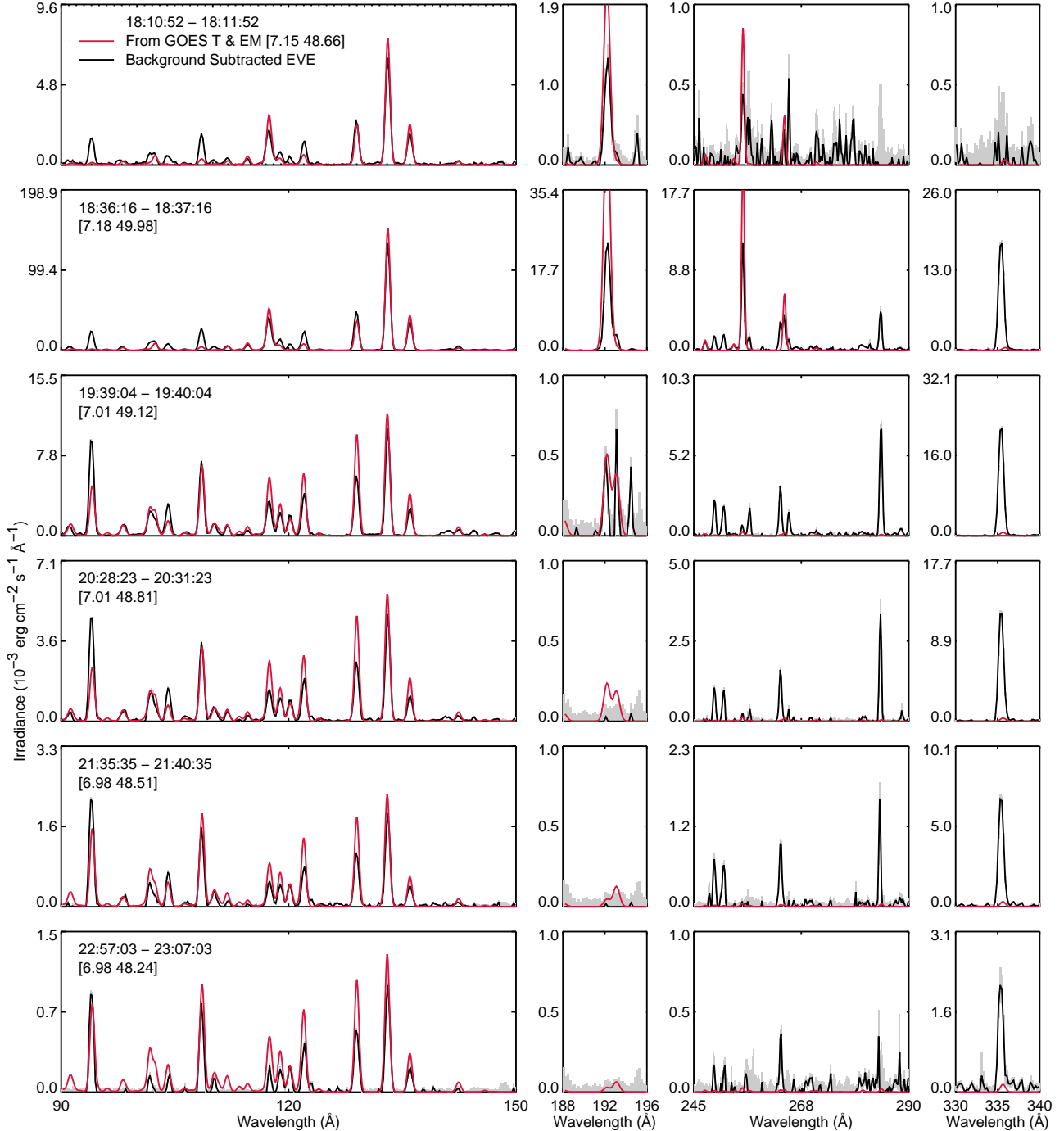


FIG. 5.— Comparison of observed EVE flare spectra with spectra inferred from the *GOES* isothermal temperature and emission at various time during the 2012 January 27 event. The grey bands indicate the statistical uncertainty in the background subtracted flare spectra. The magnitude of the *GOES* temperature and emission measure is indicated for each time interval of interest.

these measured values serve as an upper bound.

### 3.2. Isothermal Emission Measure

The *GOES* observations can be used to compute an isothermal temperature and emission measure as a function of time. This calculation is based on theoretical spectra determined from version 7 of the CHIANTI atomic database that have been convolved with the spectral responses of the two channels. Additional details on the temperatures and emission measures derived from the *GOES* observations are provided

in (White et al. 2005). To isolate the emission from the flare, pre-flare fluxes are subtracted from the observed light curves. The temperature and emission measure for this event are displayed in Figure 2. These calculations are performed using the IDL routine `goes_chianti_tem` distributed in the Solar Software Library (SSW, Freeland & Handy 1998). As has been noted in previous analyses (e.g., Sterling et al. 1997) the highest temperatures are observed before the peak in the emission measure. Here we also see that the emission mea-

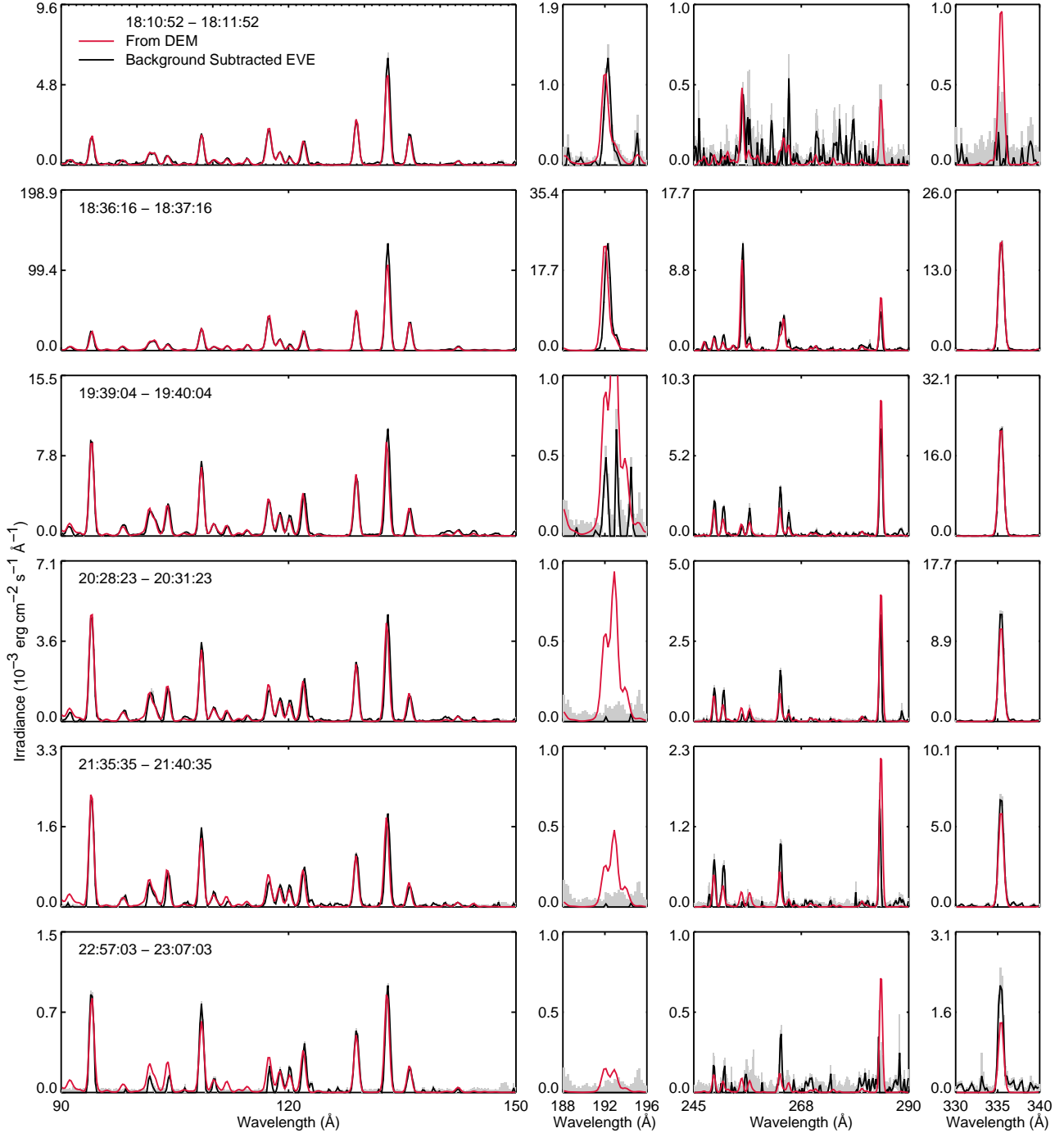


FIG. 6.— Comparison of observed EVE spectra with spectra based on a DEM model. The DEMs are shown in Figure 7.

sure decays exponentially in time while the temperature is approximately constant during the decay of the event. A relatively constant temperature evolution has been noted in previous analysis (see, for example, Doschek et al. 1980). We will return to this point in the next section.

In converting from the temperature and volume emission measure derived from *GOES* to the irradiance measured with *EVE* it is useful to recall that the irradiance is simply the intensity, or radiance, multiplied by the solid angle

$$I(\lambda) = \frac{A}{R^2} \left[ \frac{1}{4\pi} \int \epsilon(\lambda, T_e, n_e) \xi(T_e) dT_e \right], \quad (1)$$

where  $A$  is the area of the feature,  $R$  is the Earth-Sun distance,  $A/R^2$  is the solid angle, and  $\xi(T_e) = n_e^2 ds/dT$  is the line of sight DEM. Note that the spatially unresolved *GOES* observations yield a volume emission measure ( $\xi_V = A\xi(T_e)$ ) which incorporates the area factor into the line-of-sight emission measure. The isothermal *GOES* model is equivalent to a  $\delta$  function emission measure distribution

$$\xi_V(T_e) = EM_0 \delta(T_e - T_0). \quad (2)$$

To facilitate the rapid calculation of synthetic *EVE* spectra we have computed a grid of emissivities as a function of

wavelength, temperature, and density ( $\epsilon(\lambda, T_e, n_e)$ ) using the CHIANTI atomic database. We assume the CHIANTI ionization fractions and coronal abundances (Feldman et al. 1992). We interpolate on this grid to produce a spectrum at a specified temperature and density. For this work we chose a spectral binning of  $0.1 \text{ \AA}$  and convolve with a Gaussian smoothing function to account for the instrumental broadening. We find that a FWHM of  $0.7 \text{ \AA}$  best reproduces the observed line widths in MEGS-A.

In Figure 5 we compare the EVE spectra inferred from the *GOES* model with the actual observations at various times during the event. Note that no scaling factors have been applied to either the spectra inferred from *GOES* or the actual EVE observations. The wavelength range between  $90$  and  $150 \text{ \AA}$  is generally well matched by the *GOES* model. The most significant discrepancy is for the Fe XVIII emission at  $93.93$  and  $103.95 \text{ \AA}$ . Similarly, the wavelength range near  $192 \text{ \AA}$ , which contains the Fe XXIV  $192.04 \text{ \AA}$  line, is also well matched by the *GOES* model. The wavelength range between  $245$  and  $290 \text{ \AA}$  contains a mixture of high temperature flare lines, such as Fe XXIV  $255.10 \text{ \AA}$  and Fe XXIII  $263.76 \text{ \AA}$ , and lower temperature emission lines from Fe XV and Fe XVII (see, for example, Warren et al. 2008 and Del Zanna 2008 for a description of the high temperature emission in this wavelength range). In this wavelength range the *GOES* model only reproduces the highest temperature emission. Finally, we also see that the isothermal *GOES* model does not reproduce any of the observed Fe XVI  $335.41 \text{ \AA}$  irradiance. The inability of the *GOES* single temperature model to reproduce the observed EVE emission over a wide range of temperatures suggest that the flare is not isothermal.

### 3.3. Differential Emission Measure

To solve for the temperature distribution implied by the observed spectra we assume that the volume DEM can be approximated as a sum of Gaussians in log space,

$$\xi_V(T_e) = \sum_{k=1}^{N_g} EM_k \exp \left[ -\frac{(\log T_e - \log T_k)^2}{2\sigma_k^2} \right], \quad (3)$$

where the number ( $N_g$ ), position ( $\log T_k$ ), and width ( $\sigma_k$ ) of the Gaussians is fixed for a given calculation and only the magnitude of each component is varied. In general it is not possible to obtain well behaved solutions to integral equations such as Equation 1 (e.g., Craig & Brown 1976). Solutions are generally sensitive to noise and the assumption of multiple Gaussians represents an attempt to regularize or smooth the DEM while maintaining the ability to reproduce relatively isothermal distributions.

To solve for  $\xi_V(T)$  we define a temperature domain of interest  $[T_1, T_2]$  and select a value for  $N_g$ . We assume that components are equally spaced and that the width of the component is related to the width of the temperature domain by

$$\sigma_k = \sigma = \frac{\log T_2 - \log T_1}{2N_g}. \quad (4)$$

We then select initial values for  $EM_k$  and use the Levenberg-Marquardt least-squares minimization routine MPFIT to determine the values that produce the lowest value of  $\chi^2$ . In computing the differences between the spectrum computed using the emission measure model and the observed spectrum we only consider the wavelength ranges shown in Figures 5

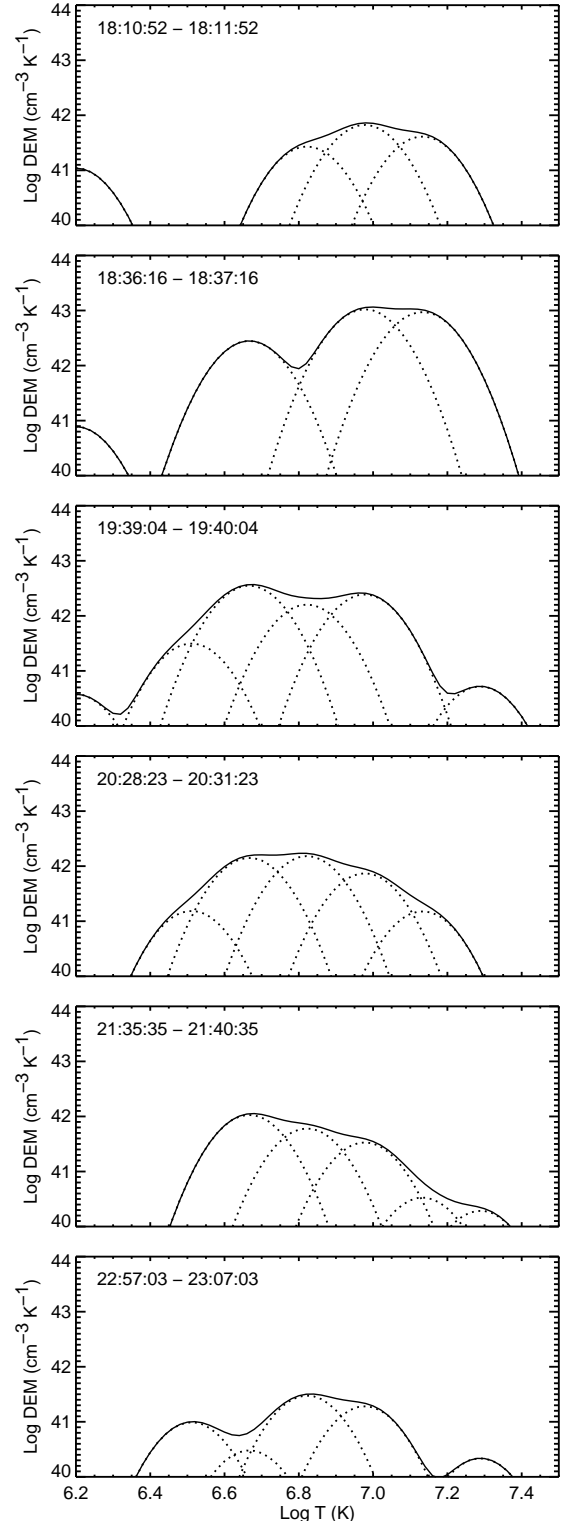


FIG. 7.— DEM distributions computed from EVE spectra taken during the 2012 January 27 event. The solid line is the actual distribution. The dotted lines indicate the contribution of each Gaussian component.

so that lines at other wavelengths, such as He II  $304 \text{ \AA}$ , do not affect the calculation.

In Figures 6 and 7 we show the EVE spectra inferred from the DEM inversion and the individual DEMs for several times

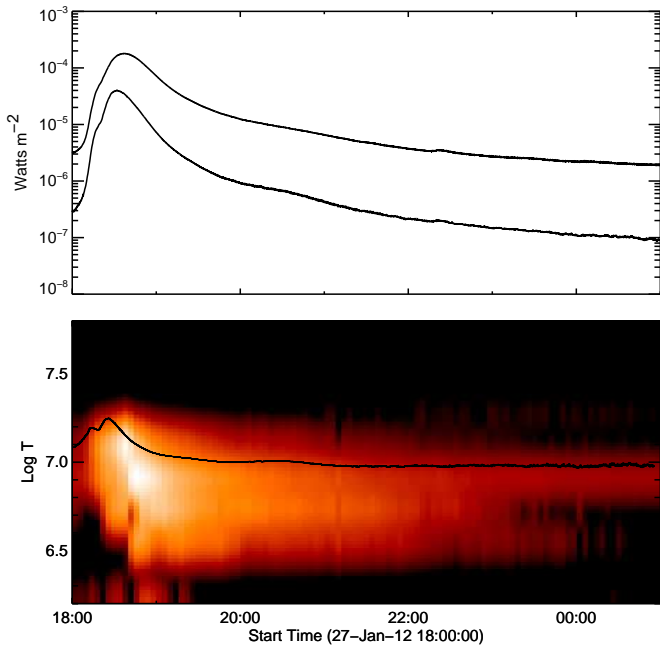


FIG. 8.— (bottom panel) The DEM distribution as a function of temperature and time derived from the EVE data. Also shown is the isothermal *GOES* temperature as a function of time. (top panel) The *GOES* soft X-ray light curves for this time period.

during the event. These calculations were performed assuming  $N_g = 10$ . We have investigated how the goodness of fit depends on the assumed number of components and found that the  $\chi^2$  declines only by a small amount for values of  $N_g$  below approximately 8 to 12. We also varied the assumed instrumental FWHM and found that a value of  $0.7 \text{ \AA}$  produces the lowest  $\chi^2$ . Finally, we also confirmed that using different values for the assumed pressure has very little influence on the goodness of fit.

For all of the spectra considered here the DEM model reproduces the observations more closely than the isothermal model does. The isothermal model produces  $\chi^2$  values that are 5–10 times higher than the DEM model, although this is due in part to absolute differences in calibration between EVE and *GOES*. The DEM model accounts for the cooler Fe XV, Fe XVI, and Fe XVIII emission lines in the observed spectra. The discrepancies between the computed and observed spectra for the higher temperature emission lines are also reduced. For the 19:39, 20:28, and 21:35 spectra, however, the DEM model appears to overestimate the observed emission near  $192 \text{ \AA}$ . Since this discrepancy is actually smaller for the *GOES* isothermal spectra, it suggests a sharp drop in the DEM above a temperature of approximately  $10^7 \text{ K}$ . Adding additional Gaussian components to the DEM, however, does not reduce the intensity of the Fe XXIV  $192.04 \text{ \AA}$  line significantly. Since this region of the spectrum is dominated by emission lines formed near 1 MK it seems likely that there actually is some Fe XXIV emission during this time, it is just difficult to observe in the pre-flare subtracted spectra. The absence of detectable emission from Ca XVII  $192.86 \text{ \AA}$ , which is formed at about  $\log T_e = 6.5$ , is consistent with this interpretation. We also note that the discrepancy between the observed spectra and the DEM model spectra for Fe XXIV  $255.10 \text{ \AA}$  line is generally small.

The selection of a limited number of intervals for considering the DEM allows us to make detailed comparisons between the modeled and observed spectra as well as with parameters inferred from the *GOES* observations. The EVE data, however, are available at a cadence of 10 s allowing the temperature evolution to be followed at high cadence over long periods of time. The isothermal temperature derived from *GOES* shown in Figure 2 suggests that analysis of high cadence data would be of interest. The isothermal model indicates a rapid increase in the temperature during the rise phase of the flare followed by a decline to a relatively constant temperature of approximately 10 MK during the decay. The DEMs shown in Figure 7 appear to be consistent with this behavior. The DEMs from 18:10 and 18:36 show considerable emission at temperatures above  $\log T_e = 7.1$ . At later times most of the emission lies at temperatures between  $\log T_e = 6.5$  and 7.1.

To compute the DEM as a function of temperature and time we divide the EVE observations during the flare into 120 s intervals and compute the DEM for each interval as described previously. In Figure 8 we show the result of this calculation. The DEM during the rise of the flare is dominated by very high temperature plasma. Near the peak of the flare the DEM becomes very broad with strong emission at temperatures between  $\log T_e = 6.4$  and 7.4. During the decay the highest temperature emission fades away as the DEM assumes an approximately constant shape. At the very end of the event the DEM at the lowest temperatures also becomes small. It seems likely, however, that this is due to the difficulty of separating the flare from the background irradiance in Fe XV  $284.16 \text{ \AA}$  and Fe XVI  $335.41 \text{ \AA}$ . As is seen in Figure 3, the AIA images from this time continue to show the formation of relatively weak post-flare loops at a wide range of temperatures.

Comparisons between the EVE DEM and the isothermal *GOES* temperature show that the evolution of the *GOES* temperature is consistent with the evolution of the DEM. These comparisons also show that the *GOES* temperature is strongly weighted towards the highest temperatures in the flare.

We have performed this time-dependent DEM calculation on 4 other long duration events that were associated with coronal mass ejections observed in AIA. The DEMs for these events are shown in Figure 9 and are generally similar to those computed for the 2012 January 27 event. All of the events that we have studied show a broad distribution of temperatures throughout the entire evolution of the flare. During the rise phase and at the peak of the events we find the highest temperatures and a rapid evolution in the DEM. During the decay we find somewhat lower peak temperatures and an approximately constant shape for the DEM.

#### 4. DISCUSSION

The combination of continuous observations, broad wavelength coverage, and relatively high spectral resolution of the EVE instrument on *SDO* provide a new opportunity to study the evolution of thermal flare plasma in detail. We have shown that these observations can be used to construct DEMs between approximately  $\log T_e = 6.3$  and 7.5. Flare related emission at lower temperatures is clearly evident in the AIA images, but it is difficult to isolate this signal in the spatially integrated irradiance observations. The highest temperature emission lines observed by EVE are from Fe XXIV, which limits the DEM at the highest temperature. EVE is unlikely to be able to detect low emission measure, “super hot” plasma ( $\log T_e > 30 \text{ MK}$ ; see, for example Caspi & Lin 2010). It



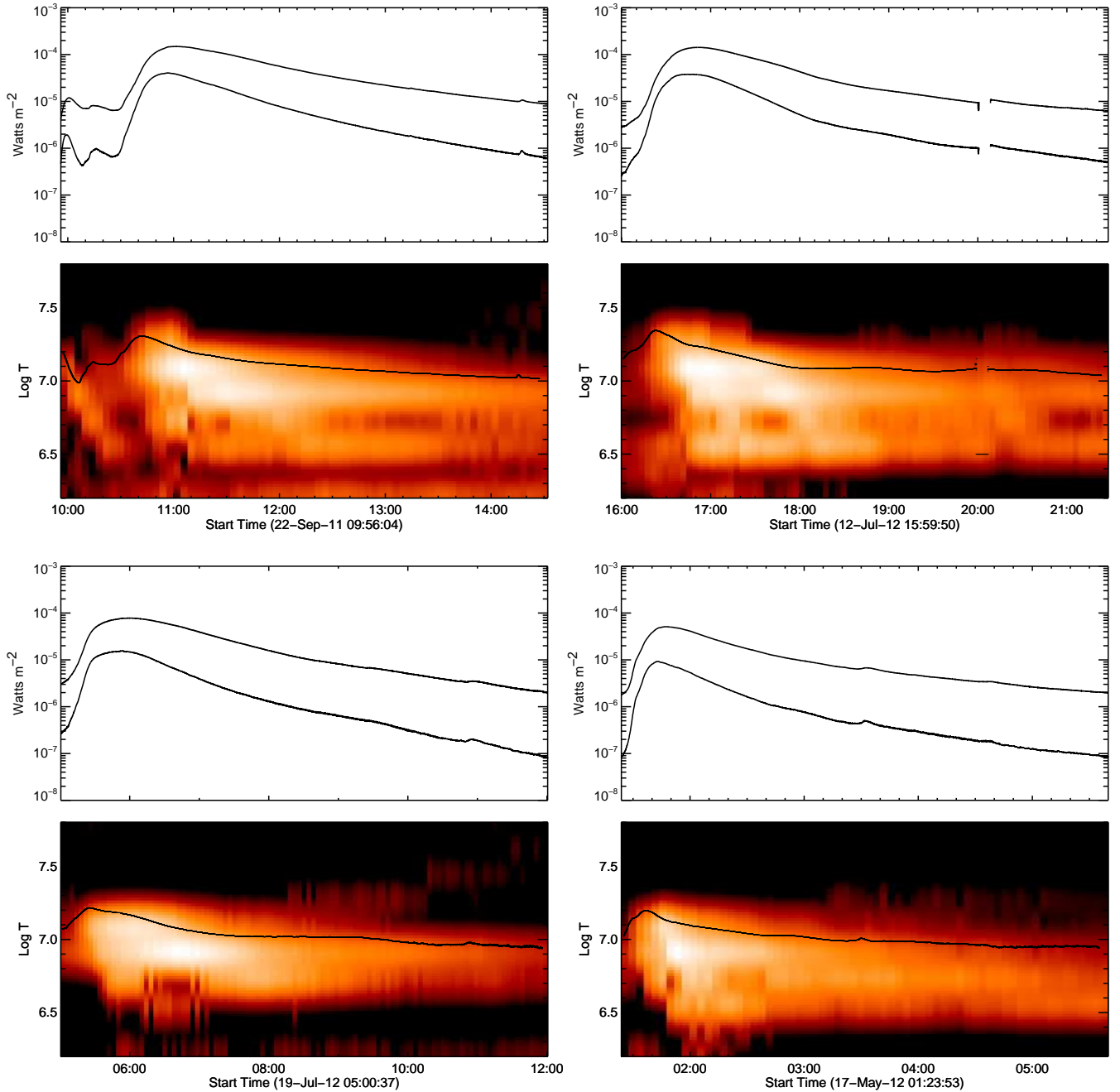


FIG. 9.— Time-dependant DEM calculations for 4 long duration events associated with coronal mass ejections. The format for each plot is the same as Figure 8.

should be possible, however, to combine the EVE data with high energy observations from RHESSI to provide a more complete description of the thermal and non-thermal emission in flares.

EVE measurements of thermal flare plasma evolution provide important constraints on theories of energy release during a flare. These observations also provide useful tests on the hydrodynamics of loop evolution. For the events considered here it is clear from both the broad temperature distributions and the AIA images showing emission over a wide range of temperatures that flares are not consistent with the evolution of a small number of loops. A more likely scenario is the continuous formation of loops that are initially heated to high

temperature and then cool. This idea of heating and cooling occurring on a succession of independently heated loops has been incorporated into simple hydrodynamic flare models that can reproduce not only the evolution of the observed intensities (Hori et al. 1997, 1998; Reeves & Warren 2002; Warren 2006; Reeves et al. 2010) but also detailed properties of the line profile (Warren & Doschek 2005). Most of this work, however, has focused on the emission at the highest temperatures as well as on the evolution of the thermal plasma during the rise and peak of an event. It remains to be seen if these models can reproduce the distribution of temperatures observed by EVE over the full evolution of a flare.

As noted in the introduction, the evolution during the ex-

tended decay of a flare holds particular promise for probing the fundamental process of magnetic reconnection. During this time we see a relatively constant shape to the emission measure over many hours. The emission measure, however, is decaying exponentially, indicating that the temperature and the density are reacting very differently to changes in the heating rate. Simple hydrodynamic arguments by Warren & Antiochos (2004) have shown that the peak density of an impulsively heated loop scales as

$$n \sim \left(\frac{E}{A}\right)^{2/3} \frac{1}{L} \quad (5)$$

while the temperature at the time of the peak density scales as

$$T \sim \left(\frac{E}{A}\right)^{1/3}, \quad (6)$$

where  $E$  is the total energy input,  $A$  is the cross-sectional

area, and  $L$  is the loop length. For the two ribbon events considered here we anticipate that the broad temperature distributions we measure will require that the flares be modeled as a succession of impulsively heated loops. Furthermore, we anticipate that over time the energy input into each loop will decline. These relationships suggest that the decline in input energy for each newly formed loop will lead to relatively large changes in the magnitude of the emission measure over time while leaving the temperature structure relatively unchanged. It remains to be demonstrated, however, that simple hydrodynamic models can reproduce the EVE observations in detail.

The *SDO* mission and this research was supported by NASA. HPW thanks Amir Caspi and Jim McTiernan for many interesting discussion on EVE flare observations.

#### REFERENCES

- Aschwanden, M. J., & Freeland, S. L. 2012, ArXiv e-prints  
 Caspi, A., & Lin, R. P. 2010, *ApJ*, 725, L161  
 Craig, I. J. D., & Brown, J. C. 1976, *A&A*, 49, 239  
 Del Zanna, G. 2008, *A&A*, 481, L69  
 Dere, K. P., & Cook, J. W. 1979, *ApJ*, 229, 772  
 Dere, K. P., Landi, E., Mason, H. E., Monsignori Fossi, B. C., & Young, P. R. 1997, *A&AS*, 125, 149  
 Dere, K. P., Landi, E., Young, P. R., Del Zanna, G., Landini, M., & Mason, H. E. 2009, *A&A*, 498, 915  
 Doschek, G. A., Feldman, U., Kreplin, R. W., & Cohen, L. 1980, *ApJ*, 239, 725  
 Feldman, U., Mandelbaum, P., Seely, J. F., Doschek, G. A., & Gursky, H. 1992, *ApJS*, 81, 387  
 Freeland, S. L., & Handy, B. N. 1998, *Sol. Phys.*, 182, 497  
 Garcia, H. A. 1994, *Sol. Phys.*, 154, 275  
 Gopalswamy, N., & Hanaoka, Y. 1998, *ApJ*, 498, L179  
 Hori, K., Yokoyama, T., Kosugi, T., & Shibata, K. 1997, *ApJ*, 489, 426  
 Hori, K., Yokoyama, T., Kosugi, T., & Shibata, K. 1998, *ApJ*, 500, 492  
 Kastner, S. O., Neupert, W. M., & Swartz, M. 1974, *ApJ*, 191, 261  
 Landi, E., Del Zanna, G., Young, P. R., Dere, K. P., & Mason, H. E. 2012, *ApJ*, 744, 99  
 Lemen, J. R., et al. 2012, *Sol. Phys.*, 275, 17  
 Mason, H. E., Doschek, G. A., Feldman, U., & Bhatia, A. K. 1979, *A&A*, 73, 74  
 McTiernan, J. M., Fisher, G. H., & Li, P. 1999, *ApJ*, 514, 472  
 Milligan, R. O., Chamberlin, P. C., Hudson, H. S., Woods, T. N., Mathioudakis, M., Fletcher, L., Kowalski, A. F., & Keenan, F. P. 2012, *ApJ*, 748, L14  
 Priest, E. R., & Forbes, T. G. 2002, *A&A Rev.*, 10, 313  
 Reeves, K. K., Linker, J. A., Mikić, Z., & Forbes, T. G. 2010, *ApJ*, 721, 1547  
 Reeves, K. K., & Warren, H. P. 2002, *ApJ*, 578, 590  
 Sterling, A. C., Hudson, H. S., Lemen, J. R., & Zarro, D. A. 1997, *ApJS*, 110, 115  
 Sui, L., & Holman, G. D. 2003, *ApJ*, 596, L251  
 Testa, P., Drake, J. J., & Landi, E. 2012, *ApJ*, 745, 111  
 Warren, H. P. 2006, *ApJ*, 637, 522  
 Warren, H. P., & Antiochos, S. K. 2004, *ApJ*, 611, L49  
 Warren, H. P., & Doschek, G. A. 2005, *ApJ*, 618, L157  
 Warren, H. P., Feldman, U., & Brown, C. M. 2008, *ApJ*, 685, 1277  
 White, S. M., Thomas, R. J., & Schwartz, R. A. 2005, *Sol. Phys.*, 227, 231  
 Woods, T. N., et al. 2012, *Sol. Phys.*, 275, 115